NASA TECHNICAL NOTE

NASA TN D-5227

NASA TN D-5227

GALVANOMAGNETIC AND THERMOMAGNETIC EFFECTS IN WHITE TIN IN FIELDS TO 3.3 TESLA AND AT TEMPERATURES BETWEEN 1.2 AND 4.2 K

by John A. Woollam

Lewis Research Center
Cleveland, Ohio

NATIONAL AERONAUTICS AND SPACE ADMINISTRATION • WASHINGTON, D. C. • MAY 1969

GALVANOMAGNETIC AND THERMOMAGNETIC EFFECTS IN WHITE TIN IN FIELDS TO 3.3 TESLA AND AT TEMPERATURES BETWEEN 1.2 AND 4.2 K

By John A. Woollam

Lewis Research Center
Cleveland, Ohio

NATIONAL AERONAUTICS AND SPACE ADMINISTRATION

For sale by the Clearinghouse for Federal Scientific and Technical Information
Springfield, Virginia 22151 – CFSTI price $3.00

ABSTRACT

The Nernst-Ettingshausen, thermoelectric power, thermal transverse-even, magnetoresistance, and Hall coefficients are measured in fields to 3.3 tesla, and at temperatures between 1.2 and 4.2 K in metallic tin. The results show that the Nernst-Ettingshausen coefficient is large, and anisotropic with respect to angle between field and crystal axes. The Nernst-Ettingshausen anistropy closely resembles that of the magnetoresistance coefficient. The temperature and field dependencies of the adiabatic coefficients are predicted from a theory for the isothermal coefficients, and these predictions are compared with experiment. Quantum oscillations in the thermoelectric power are discussed; amplitudes are in reasonably good agreement with theory.

GALVANOMAGNETIC AND THERMOMAGNETIC EFFECTS IN WHITE TIN IN FIELDS TO 3.3 TESLA AND AT TEMPERATURES BETWEEN 1.2 AND 4.2 K

by John A. Woollam

Lewis Research Center

SUMMARY

The adiabatic Nernst-Ettingshausen ϵ'_{xy}, the thermoelectric power ϵ'_{yy}, thermal transverse-even ϵ'_{zy}, magnetoresistance ρ_{yy}, and Hall ρ_{xy} coefficients are measured in magnetic fields to 3.3 tesla and for temperatures between 1.2 and 4.2 K. The results demonstrate the effects of Fermi surface topology on the Nernst-Ettingshausen coefficient. For closed electron orbits $\epsilon'_{xy} = AH^3 + BH^2$ where A and B are constants and H is field strength. For open electron orbits ϵ'_{xy} saturates to a constant value smaller than the noise level for this experiment.

The field and temperature dependencies for all the adiabatic thermomagnetic coefficients are predicted by assuming the validity of the Wiedeman-Franz law and a theory for the isothermal coefficients. The theory for the closed-orbit Nernst-Ettingshausen coefficient is in good agreement with experiment. The ϵ'_{yy} and ϵ'_{zy} coefficients do not have observable (nonoscillatory) field dependencies. This is not in agreement with predictions.

The adiabatic thermoelectric coefficient ϵ'_{yy} has strong quantum oscillations originating from the sixth-zone electron Fermi surface. The magnitudes of these oscillations are in relatively good agreement with the amplitude predicted by theory.

INTRODUCTION

It has been known for several years that open orbits have a drastic effect on magnetoresistance (refs. 1 and 2). In tin, for example, where there is compensation of electron and hole volumes, the magnetoresistance is quadratic in field for closed-orbit directions. For open orbits, the magnetoresistance saturates to a constant value (refs. 1 and 2).

Bychkov, Gurevich, and Nedlin (BGN) predict the effects of open and closed orbits on the isothermal thermoelectric tensor elements (ref. 3). One of the problems involved in a general test of the BGN theory is that none of the isothermal thermoelectric tensor elements can be determined from a single voltage measurement (refs. 4 to 6). Only at field directions parallel to axes of three-fold or higher symmetry is the measurement less than extremely tedious (refs. 4 and 5). Assuming the validity of the Wiedeman-Franz law, we resolved the problem of comparing experiment with theory, as shown in the section THEORY. In the following sections, the experimental techniques are described, the experimental results are discussed and compared with theory, and quantum oscillations in the thermoelectric power are compared with theory.

THEORY

Kinetic Equations and Transport Coefficients

The linear relations between current density $\bar{J}$, electric field $\bar{E}$, negative temperature gradient $\bar{G}$, and heat current density $\bar{w}$ may be written (refs. 4 to 6) as

$$\bar{E}^* = \hat{\rho}'\bar{J} + \hat{\epsilon}'\bar{w}^* \tag{1a}$$

$$\bar{G} = \hat{\pi}'\bar{J} + \hat{\gamma}\bar{w}^* \tag{1b}$$

or independently as

$$\bar{E}^* = \hat{\rho}\bar{J} + \hat{\epsilon}\bar{G} \tag{2a}$$

$$\bar{w}^* = -\hat{\pi}\bar{J} + \hat{\gamma}\bar{w}^* \tag{2b}$$

where

$$\bar{E}^* = \bar{E} - \frac{\nabla\mu}{e} \tag{3a}$$

$$\bar{w}^* = \bar{w} - \frac{\mu\bar{J}}{e} \tag{3b}$$

and μ is the chemical potential. (Symbols are defined in appendix A.) When J is zero, equations (1a) and (2a) give

$$\hat{\epsilon}'\bar{w}^* = \hat{\epsilon}\bar{G} \tag{4}$$

where $\hat{\epsilon}$ is the isothermal thermoelectric tensor, and $\hat{\epsilon}'$ is the adiabatic thermoelectric tensor. Equation (1b) shows that, when $J = 0$,

$$\overline{G} = \hat{\gamma}\,\overline{w}^* \tag{5}$$

so

$$\hat{\epsilon}' = \hat{\epsilon}\hat{\gamma} \tag{6}$$

where $\hat{\gamma}$ is the thermal resistivity tensor and

$$\hat{\gamma} = \hat{\lambda}^{-1} \tag{7}$$

where $\hat{\lambda}$ is thermal conductivity tensor.

Transport Coefficients in High Field Limit

Azbel', et al., (ref. 7) have shown that the asymptotic (high field limit) form of the thermal conductivity tensor $\hat{\lambda}$ is identical to the form of the electrical conductivity tensor $\hat{\sigma}$ in their field dependencies. The conditions for this to be valid are (1) thermal conduction by electrons must be much greater than conduction by phonons; (2) elastic collisions of electrons with impurities must be the dominant scattering mechanism; (3) $\omega\tau \gg 1$ where

$$\omega = \frac{eH}{m^*c} \tag{8}$$

is the cyclotron frequency, and τ is the average time between collisions. Under these conditions,

$$\hat{\lambda} = \frac{1}{3}\left(\frac{\pi k}{e}\right)^2 \hat{\sigma}T \tag{9}$$

where $\hat{\sigma}$ is the electrical conductivity tensor, and

$$L = \frac{1}{3}\left(\frac{\pi k}{e}\right)^2 \tag{10}$$

is the Lorentz ratio. It follows, by inverting equation (9), that

$$\hat{\rho} \equiv \hat{\sigma}^{-1} = TL\hat{\gamma} \tag{11}$$

and from equation (6) we get

$$\hat{\epsilon}' = \frac{\hat{\epsilon}\hat{\rho}}{LT} \tag{12}$$

Consider first the electrical resistivity tensor $\hat{\rho}$. The Lifshitz, Azbel', and Kaganov (LAK) form of $\hat{\rho}$ when $\omega\tau >> 1$ is well known, and depends on Fermi surface topology and state of compensation (refs. 1 and 2). For a compensated metal this form is

$$\hat{\rho} \sim \begin{pmatrix} H^2 & H^2 & H \\ H^2 & H^2 & H \\ H & H & H^0 \end{pmatrix} \qquad \text{Closed and compensated} \tag{13a}$$

$$\hat{\rho} \sim \begin{pmatrix} H^2 & H & H \\ H & H^0 & H^0 \\ H & H^0 & H^0 \end{pmatrix} \qquad \text{One open orbit along x axis} \tag{13b}$$

where H is the magnetic field strength. The z-azis is assumed to be in the field direction and the x-axis to be parallel to the open orbit in equation (13b).

For an uncompensated metal the resistivity tensor for closed orbits is (refs. 1 and 2)

$$\hat{\rho} \sim \begin{pmatrix} H^0 & H & H^0 \\ H & H^0 & H^0 \\ H^0 & H^0 & H^0 \end{pmatrix} \qquad \text{Closed and uncompensated} \tag{14}$$

and for one open orbit in the x-direction the tensor is the same as equation (13b).

Turning now to the BGN theory for the isothermal diffusion thermoelectric tensor, we have for a compensated metal (ref. 3)

$$\hat{\epsilon} \sim T \begin{pmatrix} H & H & H \\ H & H & H \\ H^0 & H^0 & H^0 \end{pmatrix} \qquad \text{Closed and compensated} \qquad (15a)$$

and

$$\hat{\epsilon} \sim T \begin{pmatrix} H^0 & H & H \\ H^{-1} & H^0 & H^0 \\ H^{-1} & H^0 & H^0 \end{pmatrix} \qquad \text{Open along x-direction} \qquad (15b)$$

As in the electrical case, the magnetic field is along the z-direction.

For an uncompensated metal with closed orbits the BGN theory gives (ref. 3)

$$\hat{\epsilon} \sim T \begin{pmatrix} H^0 & H^{-1} & H^0 \\ H^{-1} & H^0 & H^0 \\ H^{-1} & H^{-1} & H^0 \end{pmatrix} \qquad \text{Closed and uncompensated} \qquad (16)$$

For open orbits in uncompensated metals the thermoelectric tensor is the same as equation (15b).

For closed compensated metals we use equations (12), (13a), and (15a) to obtain the temperature and field dependence of the adiabatic thermoelectric tensor. Multiplying equation (13a) by equation (15a) gives

$$\hat{\epsilon}' \sim \begin{pmatrix} H^3 + H^2 & H^3 + H^2 & H^2 + H \\ H^3 + H^2 & H^3 + H^2 & H^2 + H \\ H^2 + H & H^2 + H & H \end{pmatrix} \qquad \text{Closed and compensated} \qquad (17)$$

It is understood in writing equation (17) that there are field- and temperature-independent coefficients multiplying each term. Thus, the ϵ'_{xy} term is understood to be of the form:

$$\epsilon'_{xy} = AH^3 + BH^2 \qquad (18)$$

where A and B are constants.

For an uncompensated metal and closed orbits we again use equation (12) to obtain $\hat{\epsilon}'$ by multiplying equation (14) by equation (16):

$$\hat{\epsilon}' \sim \begin{pmatrix} H^0 & H & H^0 \\ H & H^0 & H^0 \\ H^0 & H^0 & H^0 \end{pmatrix} \qquad \text{Closed and uncompensated} \qquad (19)$$

For the case of open orbits along the x-direction, currents along y, and field along z, the adiabatic thermoelectric tensor results from multiplying equation (13b) by equation (15b):

$$\hat{\epsilon}' \sim \begin{pmatrix} H^2 & H & H \\ H & H^0 & H^0 \\ H & H^0 & H^0 \end{pmatrix} \qquad \text{Open along the x-direction} \qquad (20)$$

If the open orbit is not mutually perpendicular to H and the currents (y-direction), equation (20) does not apply. To generalize equation (20) for the case of an open orbit at an angle α from the x-direction, a coordinate rotation is made. The rotation is in the plane perpendicular to the field. A similarity transformation of equation (20) results in

$$\hat{\epsilon}' \sim \begin{pmatrix} H^2 \cos^2\alpha + H \sin 2\alpha & H^2 \sin 2\alpha + H \cos^2\alpha + H \sin^2\alpha & H \cos \alpha \\ H^2 \sin 2\alpha + H \cos^2\alpha + H \sin^2\alpha & H^2 \sin^2\alpha + H \sin 2\alpha & H \sin \alpha \\ H \cos \alpha & H \sin \alpha & H^0 \end{pmatrix} \qquad (21)$$

Again it is understood that there are field- and temperature-independent coefficients multiplying each term in equation (21). Heat current is along y; field along z; and the open orbit makes an angle of α with the x-axis.

Tin is a compensated metal so equation (17) applies for closed orbits. The thermomagnetic coefficients measured are

(1) Adiabatic Nernst-Ettingshausen, ϵ'_{xy}

(2) Adiabatic thermoelectric, ϵ'_{yy}

(3) Adiabatic thermal transverse-even, ϵ'_{zy}

and their expected field dependencies are

$$\left.\begin{aligned}\epsilon'_{xy} &= AH^3 + BH^2 \\ \epsilon'_{yy} &= A'H^3 + B'H^2 \\ \epsilon'_{zy} &= A''H^2 + B''H\end{aligned}\right\} \quad \text{Closed orbits in tin} \tag{22}$$

where the A and B are field and temperature independent. In the presently described experiments, the open orbits are parallel to the x-direction, so equation (20) applies (see figs. 1 and 2). The expected field dependencies for tin are then

$$\left.\begin{aligned}\epsilon'_{xy} &\sim H \\ \epsilon'_{yy} &\sim H^0 \\ \epsilon'_{zy} &\sim H^0\end{aligned}\right\} \quad \text{Open orbits in tin} \tag{23}$$

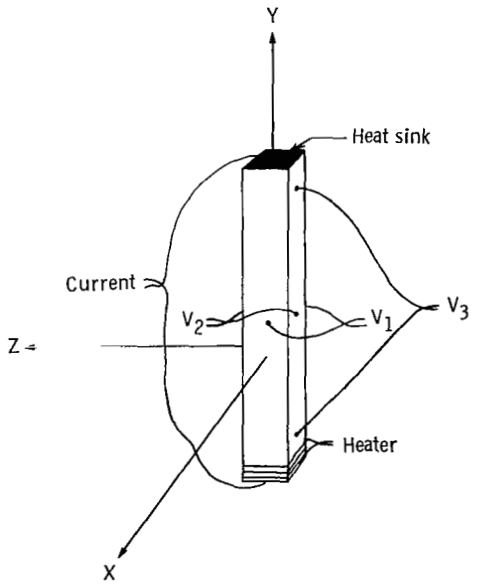

Figure 1. - Experimental sample geometry and coordinate system.

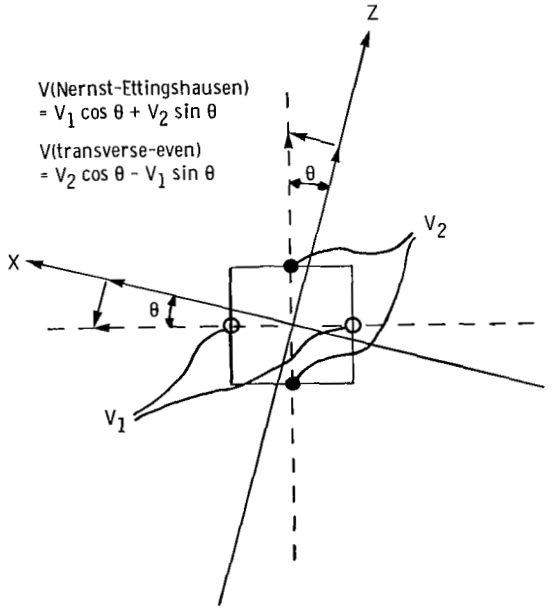

Figure 2. - Vector resolution of measured voltages V_1 and V_2 into Nernst-Ettingshausen and transverse-even components for arbitrary angle θ between field and crystal axes.

TABLE I. - PREDICTED AND MEASURED FIELD DEPENDENCIES OF ADIABATIC THERMOMAGNETIC COEFFICIENTS ϵ'_{xy}, ϵ'_{yy}, AND ϵ'_{zy}

Coefficient	Closed orbits		Open orbits	
	Theory	Experiment	Theory	Experiment
Nernst-Ettingshausen, ϵ'_{xy}	$H^3 + H^2$	$H^3 + H^2$	H^1	Smaller than noise
Thermoelectric, ϵ'_{yy}	$H^3 + H^2$	Quantum oscillations only	H^0	Smaller than noise
Transverse-even, ϵ'_{zy}	$H^2 + H^1$	Smaller than noise	H^0	Smaller than noise

These predictions, along with experimental results, are summarized in table I.

Phonon drag is not treated since it is probably very small, especially at 1.2 K. Van Baarle, et al., have measured the phonon drag contribution to be less than about 5 percent at 1.2 K for ~99.9-percent-pure tin (ref. 8).

EXPERIMENTAL APPARATUS AND PROCEDURE

The samples used in these experiments had $R_{300}/R_{4.2}$ approximately equal to 20 000. The crystal used for most measurements was in the shape of a bar 0.00318 by 0.00318 by 0.0222 meter, oriented with the [001] axis parallel to the long dimension. The perpendiculars to the 0.00318- by 0.0222-meter surfaces were along [100] equivalent directions. This crystal was grown from 99.9999-percent-pure tin, and spark cut to within 1° of the specified orientation. The sample geometry and coordinate system are shown in figure 1.

Great care was taken to attach the leads to the center of the faces, and to have a small contact area. This was done by coating the crystal with varnish, then scratching away a small contact point to which the leads were soldered. The varnish was then dissolved away. Leads were attached at the points indicated in figures 1 and 2.

Heat flow was provided by a 300-ohm-per-foot wire heater which had a total resistance of 2050 ohms, independent of temperature and magnetic field to a few percent. For thermal measurements, a constant heat flow was provided by the heater, and the

adiabatic coefficients were measured as a function of magnetic field strength, field orientation, and temperature. Potentials were measured with a dc voltmeter, and short-term noise was typically on the order of 5×10^{-8} volt.

Current leads were attached only for electrical resistance measurements, and magnetoresistance voltages were measured at pair 3 in figure 1. For the thermomagnetic coefficients, the current leads were removed so that these relatively large copper leads would not conduct heat from the sample. The thermomagnetic coefficients were measured with the sample in vacuum. One end of the sample was maintained at helium bath temperature. Adiabatic thermoelectric voltages were measured at pair 3 (fig. 1). The adiabatic Nernst-Ettingshausen ϵ'_{xy} and thermal transverse-even ϵ'_{zy} coefficients were calculated from a measurement of both V_1 and V_2 (fig. 2). For $\overline{J} = 0$, equation (1a) becomes

$$\overline{E} = \hat{\epsilon}'\overline{w} \tag{24}$$

The heat current was along the y-axis so

$$\left.\begin{aligned} E_x &= \epsilon'_{xy} w_y \\ E_y &= \epsilon'_{yy} w_y \\ E_z &= \epsilon'_{zy} w_y \end{aligned}\right\} \tag{25}$$

Power input was typically 10^{-3} watt. The Nernst-Ettingshausen voltages were calculated from

$$V(\text{Nernst-Ettingshausen}) = |V_1 \cos\theta| + |V_2 \sin\theta| \tag{26}$$

and transverse-even voltages were calculated from

$$V(\text{transverse-even}) = |V_2 \cos\theta| - |V_1 \sin\theta| \tag{27}$$

which are simply the vector components perpendicular and along the field direction. The angle between the field and the normal to the sample face θ is shown in figure 2. For rotations at fixed field, measurements were made every degree, and the coefficients ϵ'_{xy} and ϵ'_{zy} were calculated by computer using equations (26) and (27). Magnetic field direction reversals were made and coefficients averaged. Thus, final data covered $\pm90^{\circ}$. The measurements were made using number 38 copper lead wires, and

copper thermoelectric properties were assumed to be field independent and negligible compared with those of tin (ref. 5).

The magnet was a superconducting transverse split pair on an iron core with a maximum field of 3.3 tesla. Angles were read to within $\pm 0.1^{\circ}$. The temperature could be varied from 4.2 to 1.2 K by pumping on the helium bath.

A heat pulse method was frequently used and was found to give a larger signal to noise ratio than dc methods. A low-frequency heat pulse was sent to the end of the sample (fig. 1), and thermomagnetic potentials were measured by a lock-in amplifier. The method was especially useful for studying quantum oscillations.

EXPERIMENTAL RESULTS

Electrical Resistivity

The magnetoresistance of tin is plotted in figure 3 as a function of angle at a fixed field of 3.3 tesla. The Fermi surface of tin has been studied extensively (refs. 9 to 14). Results show open orbits along the [110] and [100] equivalent crystal directions. Tin is a compensated metal, and open orbits cause a saturation of the magnetoresistance as predicted by equation (13b). As shown in figure 3, saturation is found at the [110] ($\pm 45^{\circ}$) and [100] (0° and $\pm 90^{\circ}$) equivalent directions. The dip at [110] is very narrow and shows that the region of open orbits perpendicular to this field direction (also [110] orbits) is very narrow.

The magnetoresistance as a function of field for the selected field directions indi-

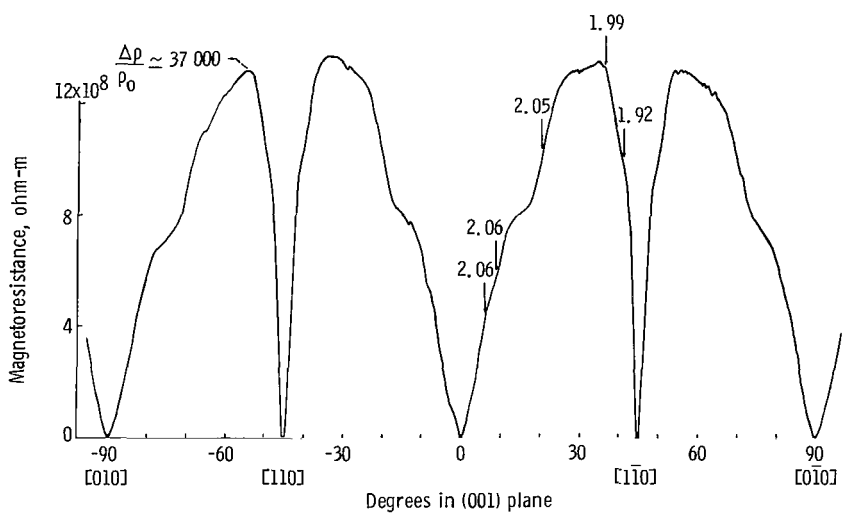

Figure 3. - Magnetoresistance at 1.2 K and 3.3 tesla for the (001) rotation plane of tin. Numbers indicated by arrows are values of n, where $\rho(H) \sim H^n$.

cated in figure 3 increases as

$$\rho_{yy} \sim H^n \tag{28}$$

For fields as low as a few tenths of tesla, up to the maximum field, n ranged from 1.92 to 2.06 as marked by arrows in figure 3, which is within experimental error of being n = 2.0 as predicted by equation (13a) (refs. 1 and 2).

The zero field electrical resistivity was measured as a function of temperature from 4.2 K to the superconducting transition at 3.7 K by an ac method (ref. 15). The resistivity at H = 0 and T = 4.2 K was 6.5×10^{-12} ohm-meter, and $R_{300}/R_{4.2} = 20\ 000$. The resistivity decreased monotonically to 4.9×10^{-12} ohm-meter at 3.7 K with $R_{300}/R_{3.7} = 27\ 000$. Thus, the sample between 4.2 and 3.7 K was not in the residual resistance region. This agrees with the published data for pure tin (ref. 16) and with the temperature dependence of ρ_{yy} at H = 3.3 tesla to be discussed in section Temperature Dependence of Nernst-Ettingshausen Coefficient, and Electrical Magnetoresistance.

The maximum $[\rho_{yy}(H) - \rho_{yy}(H=0)]/\rho_{yy}(H=0)$ at 4.2 K was 13 000 at 3.3 tesla. To first approximation

$$(\omega\tau)^2 \sim \frac{\rho_{yy}(H) - \rho_{yy}(H=0)}{\rho_{yy}(H=0)} \tag{29}$$

so $\omega\tau \sim 110$ at 4.2 K (refs. 1 and 2). An extrapolated zero field resistivity to 1.2 K results in a maximum of approximately $[\rho_{yy}(H) - \rho_{yy}(H=0)]/\rho_{yy}(H=0)$ of 37 000 as noted in figure 3. This makes $\omega\tau \sim 190$ at 1.2 K.

Thermomagnetic Results

The results of the adiabatic Nernst-Ettingshausen ϵ'_{xy} and thermal transverse-even ϵ'_{zy} coefficients calculated from experimental data are shown in figure 4. Equations (17) and (22) and table I show that for closed orbits ϵ'_{xy} should have a field dependence which has cubic and quadratic terms in H. Field sweeps were made at many angles, and all showed the predicted $\epsilon'_{xy} = AH^3 + BH^2$ dependence. The values of A and B depended on angle.

A plot of ϵ'_{xy}/H^2 against H is a straight line for fields below about 2.0 tesla (fig. 5). Figure 5 shows that only a quadratic term remains above 2.0 tesla, and by 3.3 tesla the field dependence of ϵ'_{xy} has diminished even further. The probable explanation for the results above 2.0 tesla is that the Wiedeman-Franz law (eq. (9)) is

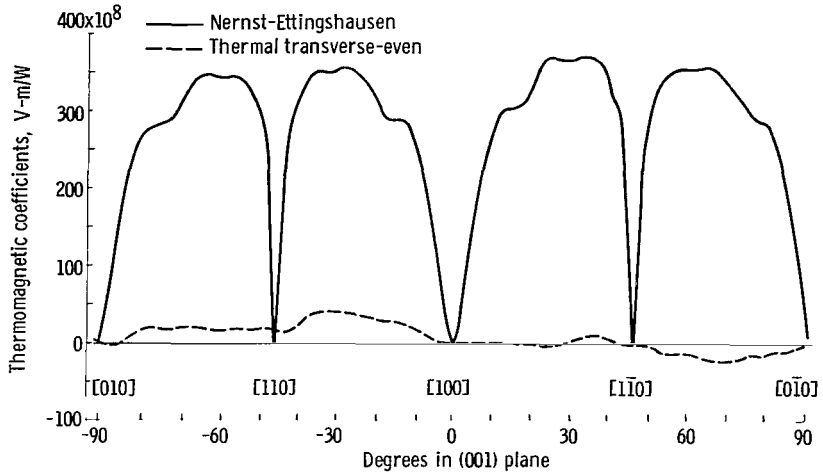

Figure 4. - Adiabatic Nernst-Ettingshausen ϵ'_{xy}, and thermal transverse-even ϵ'_{zy} coefficients for (001) rotation plane of tin at 3.3 tesla and at 1.2 K, demonstrating effects of Fermi surface topology on ϵ'_{xy}.

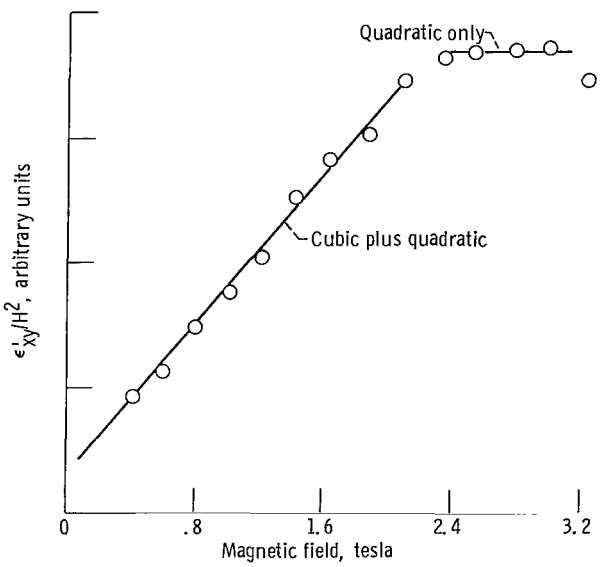

Figure 5. - Measured field dependence of adiabatic Nernst-Ettingshausen coefficient ϵ'_{xy}/H^2 at 1.2 K and $\theta = 30°$.

no longer valid. Heat conduction is by electrons and phonons, and high fields decrease the electronic thermal conduction until phonon conduction becomes important. By the Wiedeman-Franz law and equation (13a), the electronic thermal resistivity increases as H^2 for closed orbits. At high fields, where lattice conduction is important, the field dependence of the thermal resistivity diminishes. At high enough fields, the thermal resistivity $\hat{\gamma}$ becomes independent of field, and equations (11) and (12) indicate a lower field dependence for ϵ' as a result (ref. 4).

Equations (20) and (23) predict the field dependence of ϵ'_{xy} for open orbits in tin to be H, as opposed to H^3 and H^2 for closed orbits. This predicts dips in ϵ'_{xy} at open-orbit directions. Within experimental limits, ϵ'_{xy} was found to go to zero at the open-orbit directions [110] and [100], as shown in figure 4. If there is an H dependence at these angles, it is very weak.

Equations (20) and (23) predict that the thermoelectric and thermal transverse-even coefficients ϵ'_{yy} and ϵ'_{zy} go to zero at open-orbit directions. This is experimentally observed. However, equations (17) and (22) predict strong field dependencies of ϵ'_{yy} and ϵ'_{zy} for closed-orbit field directions. This was not observed experimentally. Figure 4 shows that ϵ'_{zy} was within experimental limits of being zero for all angles. The large scatter of data about $\epsilon'_{zy} = 0$ in figure 4 results from ϵ'_{zy} being the difference between two rather large numbers (see eq. (28)). The error in each one is approximately $\pm 25 \times 10^{-8}$ volt-meter per watt, and the scatter in ϵ'_{zy} fits approximately within $\pm 50 \times 10^{-8}$ volt-meter per watt.

Figure 6 shows the adiabatic thermoelectric coefficient ϵ'_{yy} as a function of angle in the (001) plane at 3.3 tesla. The nonoscillatory field dependence has a maximum value of 2.5×10^{-8} volt-meter per watt and is caused entirely by a 0.025-millimeter misalinement of the V_3 contact points from the vertical. This nonoscillatory dependence of ϵ'_{yy} on angle reverses sign on reversing field direction and is due to a small component of the Nernst-Ettingshausen voltage. Within limits of experimental error, the ϵ'_{yy} nonoscillatory field dependence is zero for all angles in the (001) plane. The oscillatory part of ϵ'_{yy} is discussed in the QUANTUM OSCILLATIONS IN THERMOELECTRIC COEFFICIENT ϵ'_{yy} section.

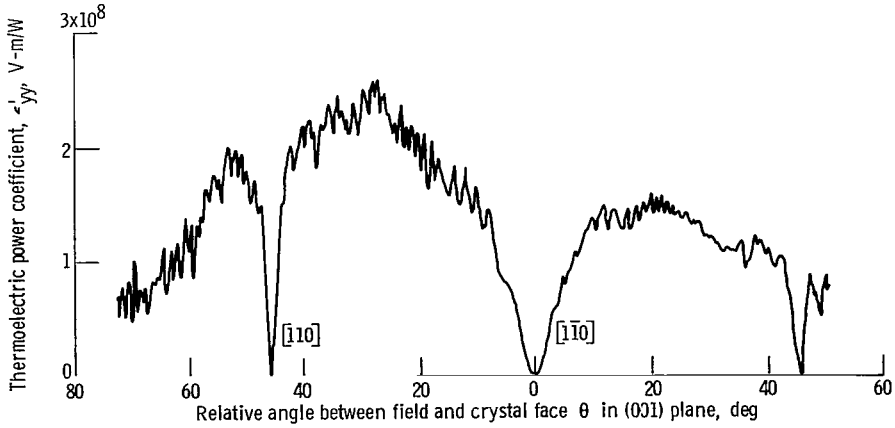

Figure 6. - Adiabatic thermoelectric coefficient ϵ'_{yy} at 3.3 tesla and 1.2 K, showing quantum oscillations for nearly all directions except along [110] and [100]. The nonoscillatory background is not real, as explained in text.

Temperature Dependence of Nernst-Ettingshausen Coefficient, and Electrical Magnetoresistance

The LAK and BGN theories assume that scattering is by elastic collisions only. This means the metal must be in the residual resistance region of temperature. As discussed in the section Electrical Resistivity, the present crystal of tin, as shown by zero field resistance measurements, was not in the residual resistance region between 4.2 and 3.7 K. As an additional test, the magnetoresistance at 3.3 tesla was measured as a function of temperature from 4.2 to 1.2 K, for a closed-orbit direction. The value of ρ_{yy} at 3.3 tesla increased by 50 percent in going from 4.2 to 2.0 K. Below 2.0 K, it saturated to a constant value.

The field dependence of $\hat{\rho}$ and $\hat{\epsilon}$, as described in equations (13) to (21), actually came from an expansion in terms of $\omega\tau$; that is, H is proportional to ω (eq. (8)). In the limit of only elastic scattering, τ is independent of temperature. In the present crystal of tin, the increase of 50 percent in the resistance at 3.3 tesla is due to an increase in τ. Below about 1.8 K, the crystal is in the residual resistance region, τ is constant, and there is no further increase in the magnetoresistance.

From equation (12),

$$\hat{\epsilon}' = \frac{\hat{\epsilon}\hat{\rho}}{LT} \tag{12}$$

and equation (15) shows that $\hat{\epsilon}$ is proportional to T. Thus, if $\hat{\rho}$ and $\hat{\epsilon}/T$ are independent of temperature,

$$\hat{\epsilon}' \sim T^{0} \tag{30}$$

Equation (30) is the temperature dependence in the residual resistance region only. This explains the saturation of ϵ_{xy} to a constant value below about 1.6 K (fig. 7). The increase in ϵ_{xy} with decreasing temperature between 4.2 and 1.8 K is due at least partially to the increase in τ, which results from a decrease in electron-phonon scattering.

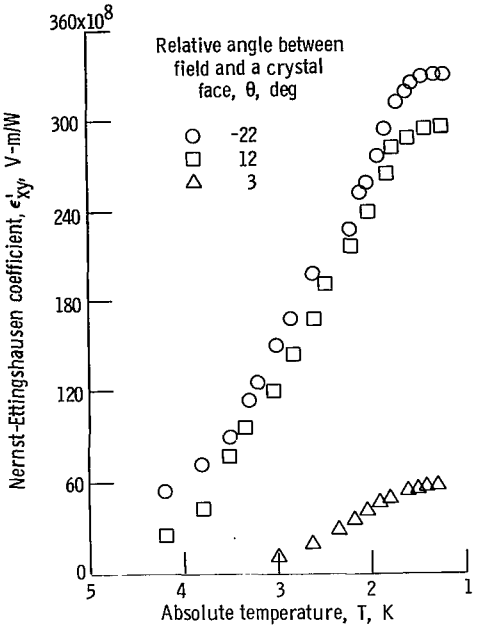

Figure 7. - Temperature dependence of adiabatic Nernst-Ettingshausen coefficient for field of 3.3 tesla.

QUANTUM OSCILLATIONS IN THERMOELECTRIC COEFFICIENT ϵ'_{yy}

Strong quantum oscillations in the adiabatic thermoelectric coefficient ϵ'_{yy} were observed that had amplitudes up to $\sim 0.5\times10^{-8}$ volt-meter per watt at 3.3 tesla. By rotating the crystal in a fixed field of 3.3 tesla, oscillations were seen at nearly all angles except near [110] and [100] equivalent symmetry directions (fig. 6). These oscillations arise because of the quantization of electron motion in a plane perpendicular to the applied magnetic field. (Reference 17 gives a background on this phenomenon.) As shown in a theory by Horton, the thermoelectric coefficient ϵ''_{yy} should depend approximately on field and angle (ref. 18), and

$$\epsilon'_{yy} \sim A_1 \sin\left(\frac{2\pi F(\theta)}{H} + \gamma\right) \tag{31}$$

where A_1 is the amplitude, $F(\theta)$ is the deHaas-van Alphen frequency, H is the field, θ is the relative direction of field with respect to crystal axes (fig. 2), and γ is a phase factor. Equation (31) shows that ϵ'_{yy} is periodic in $1/H$ with frequency $F(\theta)$. The frequency $F(\theta)$ is a large number and has a strong dependence on θ. Therefore, ϵ'_{yy} also oscillates as θ changes when H is fixed. Experimental measurements give

$F(\theta)$, which is proportional to the extremal cross-sectional area of the Fermi surface perpenducular to the θ-direction.

The presently observed oscillations have a frequency $F(\theta)$ characteristic of the sixth-zone electron surface section (refs. 9 to 14). However, at an angle $16^{o} \pm 5^{o}$ from [110], a large amplitude oscillation of frequency 0.22×10^{3} tesla (0.22×10^{7} gauss) is observed. This frequency is more than a factor of 2 lower than any reported frequency in this rotation plane (refs. 9 to 14). The origin of the lower frequency oscillations is presently not understood.

Horton calculates the "absolute" thermoelectric tensor which from definition is (refs. 4 to 6, and 18)

$$\hat{\epsilon}'' = \hat{\sigma}\hat{\epsilon}'\hat{\lambda} \tag{32}$$

$$\hat{\epsilon}' = \hat{\rho}\hat{\epsilon}''\hat{\gamma}$$

or

$$\hat{\epsilon}' = \frac{\hat{\rho}}{LT}\hat{\epsilon}''\hat{\rho} \tag{34}$$

To evaluate equation (34) consider first the resistivity tensor $\hat{\rho}$. The Hall resistivity ρ_{xy} was measured and found to be much smaller than the resistivity ρ_{yy}, and the oscillatory parts of $\hat{\rho}$ were found to be small compared to the nonoscillatory parts. From equation (13a) the other off-diagonal terms in $\hat{\rho}$ are of low power in H, and so are neglected. Thus,

$$\hat{\rho} \simeq \begin{pmatrix} \rho_{xx} & --- & --- \\ --- & \rho_{yy} & --- \\ --- & --- & --- \end{pmatrix} \tag{35}$$

Using the appropriate numbers for tin and the Horton theory (ref. 18), $\hat{\epsilon}''$ is approximately:

$$\hat{\epsilon}'' \simeq \begin{pmatrix} \tilde{\epsilon}''_{xx} & \epsilon''_{xy} & --- \\ \epsilon''_{yx} & \tilde{\epsilon}''_{yy} & --- \\ --- & --- & --- \end{pmatrix} \tag{36}$$

Using equations (34) to (36), and taking only the oscillatory component of ϵ'_{yy} we get

$$\tilde{\epsilon}'_{yy} \simeq \frac{\rho^2}{LT} \tilde{\epsilon}''_{yy} \tag{37}$$

where ρ is the yy component of $\hat{\rho}$.

To apply Horton's theory, we make the following assumptions (refs. 19 and 20):

$$m \text{ is replaced by } m^* \tag{38}$$

$$n \text{ is replaced by } \frac{1}{6\pi^2}\left(\frac{2m^*\epsilon_F}{\hbar^2}\right)^{3/2} \tag{39}$$

$$\omega_c \text{ is replaced by } \frac{eH}{m^*c} \tag{40}$$

$$\mathscr{E}_F \text{ is replaced by } \hbar\omega_c \frac{F}{H} \tag{41}$$

where all terms have their usual meaning, and F is the de Haas-van Alphen frequency. Horton's unaltered expression is

$$\tilde{\epsilon}''_{yy} = -\frac{2\pi^2}{3}\frac{ne}{m}\frac{k^2T}{\mathscr{E}_F}\frac{1}{\tau}\frac{1}{\omega^2}\left[1 - \frac{15\sqrt{2}}{8\pi^2}\frac{\sqrt{\hbar\omega\mathscr{E}_F}}{kT}\sum_{\nu}\frac{(-1)^\nu}{\sqrt{\nu}}A_3(\lambda)\sin b\right.$$

$$\left. + \frac{45\sqrt{2}}{8\pi^2}\sqrt{\frac{\hbar\omega}{\mathscr{E}_F}}\sum_{\nu}\frac{(-1)^\nu}{\sqrt{\nu}}A_4(\lambda)\cos b\right] \tag{42}$$

when $\omega\tau >> 1$. Evaluating the magnitude of the sin b and cos b terms for tin shows that the term in sin b is much larger than the term in cos b and also much greater than 1. The $\nu = 1$ term dominates the terms with $\nu > 1$. Equation (42) thus reduces to

$$\tilde{\epsilon}''_{yy} \simeq \frac{5}{6\pi^2}\frac{ke^{3/2}}{\hbar^{3/2}c^{1/2}}\frac{F}{H^{1/2}}\frac{1}{\omega\tau}A_3(\lambda)\sin b \tag{43}$$

and from equation (40),

$$\tilde{\epsilon}'_{yy} \simeq \frac{\rho(H)^2}{2} \frac{5}{6\pi^2} \frac{ke^{3/2}}{\hbar^{3/2} c^{1/2}} \frac{F}{H^{1/2}} \frac{1}{\omega\tau} A_3(\lambda) \sin b \tag{44}$$

where $A_3(\lambda)$ and $\sin b$ are discussed below. Evaluating equation (44) at 1.2 K gives

$$\tilde{\epsilon}'_{yy} \simeq \frac{\rho^2(H)}{\omega\tau} \frac{F}{H^{1/2}} 2.315 \times 10^{26} A_3(\lambda) \sin b \tag{45}$$

For sixth-zone oscillations in tin,

$$\tilde{\epsilon}'_{yy} \simeq 5.7 \times 10^{-8} A_3(\lambda) \sin b \qquad \text{volt-meter/watt} \tag{46}$$

where

$$\left.\begin{aligned} A_3(\lambda) &= -\pi \operatorname{csch}(\lambda)(1 - \lambda \operatorname{ctnh} \lambda) \\ \lambda &= 2\pi^2 \frac{kT}{\hbar\omega} \\ b &= \frac{2\pi F}{H} - \frac{\pi}{4} \end{aligned}\right\} \tag{47}$$

and $A_3(\lambda)$ is a maximum when $\lambda = 1.67$. This occurs at 1.2 K for sixth-zone orbits in tin. The maximum value of $A_3(\lambda)$ is -1. Thus, equation (46) is

$$\tilde{\epsilon}'_{yy} \simeq 5.7 \times 10^{-8} \sin\left(\frac{2\pi F}{H} - \frac{\pi}{4}\right) \qquad \text{volt-meter/watt} \tag{48}$$

The Horton theory and equations (42) to (48) are for a free electron Fermi sphere. To predict the amplitude for the sixth-zone Fermi surface section, the theoretical expression must be corrected. Therefore, equation (48) is multiplied by the ratio of the effective number of carriers on the sixth zone to the effective number of carriers on the free electron sphere for any particular field direction. The number of carriers effective is proportional to the distance in momentum space parallel to the field, in which all electrons have very nearly the same orbit radii. This is proportional to the Fermi sur-

face curvature parallel to the field. The curvature correction is therefore (refs. 19 and 21)

$$C = \left[\frac{\left(\frac{\partial^2 A}{\partial k_z^2} \right)_{\text{free electron}}}{\frac{\partial^2 A}{\partial k_z^2}} \right]^{1/2} \tag{49}$$

where A is the extremal cross-sectional area perpendicular to the field. For a free electron sphere,

$$\frac{\partial^2 A}{\partial k_z^2} = 2\pi \tag{50}$$

The denominator in equation (49) is given approximately by (refs. 19 and 20)

$$\left(\frac{\partial^2 A}{\partial k_z^2} \right)_{k_o} = \frac{2\sqrt{2}\,\pi \left(\frac{e}{\hbar c} \right)^{1/2} F^{1/2}}{\left(3\pi^2 n_o \right)^{1/3}} \tag{51}$$

where n_o is the electron density and F is the de Haas-van Alphen frequency. Evaluating equations (51) and (49) for the sixth zone of tin gives

$$C = 3.59 \tag{52}$$

The second factor relating the number of effective carriers on the sixth zone to the free electron sphere is the circumference at the extremal cross section perpendicular to the field. Using Gold and Priestley's free electron radius (ref. 9), the ratio of the sixth-zone circumference (with $\overline{H}$ 22^o from [110] in (001)) to the free electron circumference is approximately

$$\frac{\text{Sixth-zone circumference}}{\text{Free electron circumference}} \simeq 0.071 \tag{53}$$

The theoretical amplitude (eq. (48)) is thus multiplied by equations (52) and (53) to give

$$\tilde{\epsilon}'_{yy} \text{ (theory)} \simeq 1.5\times10^{-8} \text{ volt-meter/watt} \tag{56}$$

The experimentally observed amplitude was

$$\tilde{\epsilon}'_{yy} \text{ (experiment)} \simeq 0.3\times10^{-8} \text{ volt-meter/watt} \tag{56}$$

The agreement between theory and experiment is therefore reasonably good.

Agreement between theory and experiment would be somewhat better if the thermal resistivity were used in evaluating equations (33) and (34) rather than using the Wiedeman-Franz law to relate the thermal and electrical resistivities. As discussed in the section Thermomagnetic Results, the thermal resistivity does not continue increasing quadratically as predicted by the Wiedeman-Franz law and equation (13a). The field dependence of $\tilde{\epsilon}'_{yy}$ (eq. (41)) would be smaller than predicted from a ρ^2 dependence. This would reduce the theoretical amplitude predicted by equation (54)

The relatively good agreement between theory and experiment supports the use of equation (37) and the assumptions leading to it. It also shows that the Horton free electron theory and the assumption of randomly located neutral point impurities were reasonably good.

CONCLUSIONS

The adiabatic Nernst-Ettingshausen coefficient ϵ'_{xy}, the thermoelectric coefficient ϵ'_{yy}, and the thermal transverse-even coefficient ϵ'_{zy} are measured in magnetic fields to 3.3 tesla and temperatures between 1.2 and 4.2 K. The results clearly demonstrate the effect of Fermi surface topology on ϵ'_{xy}, which is very anistropic with respect to the angle between field and open-orbit directions. This anisotropy is very similar to the anisotropy in the electrical magnetoresistance.

The field and temperature dependence for all of the adiabatic thermomagnetic coefficients are predicted by assuming the validity of the Wiedeman-Franz law and a theory for the isothermal coefficients. For closed-orbit directions, the field dependence of ϵ'_{xy} is $AH^3 + BH^2$, in agreement with predictions. The temperature dependence of ϵ'_{xy} below 1.6 K is in agreement with predictions.

The adiabatic thermoelectric coefficient ϵ'_{yy} has strong quantum oscillations

originating from the sixth-zone electron Fermi surface. The magnitude of these oscillations is in relatively good agreement with the amplitude predicted by theory.

Lewis Research Center,
National Aeronautics and Space Administration,
Cleveland, Ohio, February 24, 1969,
129-02-05-14-22.

APPENDIX - SYMBOLS

A	cross-sectional area of Fermi surface
A_1	amplitude of oscillatory effect
A, B, A', B', A'', B''	constants independent of field and temperature, but dependent on angle between field and crystal axes
$A_3(\lambda), A_4(\lambda)$	parameters dependent on ω and T
b	parameter, $(2\pi F/H) - (\pi/4)$
c	velocity of light
$\overline{E}$	electric field vector
$\overline{E}^*$	experimental electric field vector, $\overline{E} - \nabla\mu/e$
e	charge on an electron
E_x, E_y, E_z	components of E vector in Cartesian coordinates
$\mathscr{E}_F$	Fermi energy
$F(\theta)$	de Haas-van Alphen frequency
$\overline{G}$	negative temperature gradient vector
H	magnetic field strength
$\overline{H}$	vector magnetic field
$\hbar$	Planck's constant divided by 2π
$\overline{J}$	electric current density vector
k	Boltzmann constant
L	Lorentz ratio from Wiedeman-Franz law
m	electron mass
m*	effective mass
n	density of electrons
$\overline{p}$	crystal momentum
R	electrical resistance with $\overline{J}$ parallel to [001]
R(H)	Hall resistivity
T	absolute temperature
V_1, V_2, V_3	experimentally measured potentials

w_x, w_y, w_z	components of $\overline{w}$ vector in Cartesian coordinates
$\overline{w}$	heat current density vector
$\overline{w}^*$	modified heat current density, $\overline{w} - \mu\overline{J}/e$
α	angle between open orbit and x-direction
α_{ij}	components of $\hat{\rho}$ tensor which are linear in H
β	constant
γ	phase factor
$\hat{\gamma}$	adiabatic thermal resistivity tensor
$\hat{\epsilon}$	isothermal thermoelectric tensor
$\hat{\epsilon}'$	adiabatic thermoelectric tensor
$\hat{\epsilon}''$	absolute thermoelectric tensor
$\tilde{\epsilon}'$	oscillatory part of adiabatic thermoelectric tensor
$\tilde{\epsilon}''$	oscillatory part of isothermal thermoelectric tensor
$\tilde{\epsilon}''_{yy}$	oscillatory part of isothermal thermoelectric power coefficient
$\tilde{\epsilon}''_{xy}$	oscillatory part of isothermal Nernst-Ettingshausen coefficient
$\tilde{\epsilon}'_{yy}$	oscillatory part of adiabatic thermoelectric power coefficient
$\tilde{\epsilon}'_{xy}$	oscillatory part of adiabatic Nernst-Ettingshausen coefficient
θ	relative angle between field and crystal face
λ	parameter, $2\pi^2 kT/\hbar w$
$\hat{\lambda}$	isothermal thermal conductivity tensor
μ	chemical potential
ν	integers from 1 to ∞
$\hat{\pi}$	isothermal peltier tensor
$\hat{\pi}'$	adiabatic peltier tensor
ρ	transverse or ρ_{yy} component of $\hat{\rho}$ tensor
ρ_{xy}	Hall coefficient
ρ_{yy}	component of $\hat{\rho}$ tensor
$\hat{\rho}$	isothermal electrical resistivity tensor
$\hat{\rho}'$	adiabatic electrical resistivity tensor

$\hat{\sigma}$	electrical conductivity tensor
τ	average time between elastic scattering
ω	cyclotron frequency, eH/m*c
[100], [110], [001]	crystal axes specified by Miller indices

REFERENCES

1. Lifshitz, I. M.; Azbel', M. Ia.; and Kaganov, M. I.: The Theory of Galvanomagnetic Effects in Metals. Soviet Phys. JETP, vol. 4, no. 1, Feb. 1957, pp. 41-54.

2. Fawcett, E.: High-Field Galvanomagnetic Properties of Metals. Advances in Phys., vol. 13, 1964, pp. 139-191.

3. Bychkov, Yu. A.; Gurevich, L. É.; and Nedlin, G. M.: Thermoelectric Phenomena in Strong Magnetic Fields in Metals Possessing Various Fermi Surfaces. Soviet Phys. JETP, vol. 10, no. 2, Feb. 1960, pp. 377-380.

4. Long, J. R.; Grenier, C. G.; and Reynolds, J. M.: Electron and Lattice Transport Phenomena in an Antimony Crystal at Liquid - He^4 Temperatures. Phys. Rev., vol. 140, no. 1A, Oct. 4, 1965, pp. 187-201.

5. Grenier, C. G.; Reynolds, J. M.; and Zebouni, N. H.: Electron Transport Phenomena in Zinc at Liquid-Helium Temperatures. Phys. Rev., vol. 129, no. 3, Feb. 1, 1963, pp. 1088-1104.

6. Jan, J. P.: Galvano-and Thermomagnetic Effects in Metals. Solid State Physics. Vol. 5. Academic Press, Inc., 1957, pp. 1-96.

7. Azbel', M. Ia.; Kaganov, M. I.; and Lifshitz, I. M.: Thermal Conductivity and Thermoelectric Phenomena in Metals in a Magnetic Field. Soviet Phys. JETP, vol. 5, no. 5, Dec. 1957, pp. 967-970.

8. Van Baarle, C.; Cuelenaere, A. J.; Roest, G. J.; and Young, M. K.: The Anisotropy of the Thermoelectric Power of Tin at Low Temperatures. Physica, vol. 30, 1964, pp. 244-253.

9. Gold, A. V.; and Priestley, M. G.: The Fermi Surface of White Tin. Phil. Mag., vol. 5, no. 59, Nov. 1960, pp. 1089-1104.

10. Stafleu, M. D.; and de Vroomen, A. R.: The Fermi Surface of White Tin. Phys. Letters, vol. 23, no. 3, Oct. 17, 1966, pp. 179-181.

11. Alekseevskiĭ, N. E.; Gaĭdukov, Yu. P.; Lifshitz, I. M.; and Peschanskiĭ, V. G.: The Fermi Surface of Tin. Soviet Phys. JETP, vol. 12, no. 5, May 1961, pp. 837-846.

12. Khaĭkin, M. S.: Investigation of the Fermi Surface of Tin by the Method of Cyclotron Resonance. Soviet Phys. JETP, vol. 15, no. 1, July 1962, pp. 18-23.

13. Weisz, Gideon: Band Structure and Fermi Surface of White Tin. Phys. Rev., vol. 149, no. 2, Sept. 16, 1966, pp. 504-518.

14. Anderson, J. Gerald; and Young, R. C.: Magnetoresistance of Tin over a Large Range of Magnetic Fields. Phys. Rev., vol. 168, no. 3, Apr. 15, 1968, pp. 696-707.

15. Woollam, J. A.: A Simple A. C. Technique for Galvanomagnetic and Shubnikov-deHaas Measurements. Cryogenics, vol. 8, no. 5, Oct. 1968, pp. 312-313.

16. Hall, L. A.: Survey of Electrical Resistivity Measurements on 16 Pure Metals in the Temperature Range 0° to 273° K. Tech. Note 365, National Bureau of Standards (NASA CR-94169), Feb. 1968.

17. Ziman, John M.: Principles of the Theory of Solids. Cambridge University Press, 1964, p. 269.

18. Horton, Philip B.: Quantum Transport Theory of Free Electrons in a Strong Magnetic Field. Ph. D. Thesis, Louisiana State Univ., 1964.

19. Trodahl, H. J.: Quantum Oscillations in the Peltier Effect in Zinc. Ph. D. Thesis, Michigan State Univ., 1968.

20. Kittel, Charles: Quantum Theory of Solids. John Wiley & Sons, Inc., 1963, p. 220.

21. Shoenberg, D.: The De Haas-Van Alphen Effect. Progress in Low Temperature Physics. Vol. 2, C. J. Gorter, ed., Interscience Publishers, 1957, pp. 234-273.

NASA-Langley, 1969 —— 26 E-4809

NATIONAL AERONAUTICS AND SPACE ADMINISTRATION
WASHINGTON, D. C. 20546
OFFICIAL BUSINESS

FIRST CLASS MAIL

POSTAGE AND FEES PAID
NATIONAL AERONAUTICS A
SPACE ADMINISTRATION

POSTMASTER: If Undeliverable (Section 15
Postal Manual) Do Not Ret

"The aeronautical and space activities of the United States shall be conducted so as to contribute . . . to the expansion of human knowledge of phenomena in the atmosphere and space. The Administration shall provide for the widest practicable and appropriate dissemination of information concerning its activities and the results thereof."

—NATIONAL AERONAUTICS AND SPACE ACT OF 1958

NASA SCIENTIFIC AND TECHNICAL PUBLICATIONS

TECHNICAL REPORTS: Scientific and technical information considered important, complete, and a lasting contribution to existing knowledge.

TECHNICAL NOTES: Information less broad in scope but nevertheless of importance as a contribution to existing knowledge.

TECHNICAL MEMORANDUMS: Information receiving limited distribution because of preliminary data, security classification, or other reasons.

CONTRACTOR REPORTS: Scientific and technical information generated under a NASA contract or grant and considered an important contribution to existing knowledge.

TECHNICAL TRANSLATIONS: Information published in a foreign language considered to merit NASA distribution in English.

SPECIAL PUBLICATIONS: Information derived from or of value to NASA activities. Publications include conference proceedings, monographs, data compilations, handbooks, sourcebooks, and special bibliographies.

TECHNOLOGY UTILIZATION PUBLICATIONS: Information on technology used by NASA that may be of particular interest in commercial and other non-aerospace applications. Publications include Tech Briefs, Technology Utilization Reports and Notes, and Technology Surveys.

Details on the availability of these publications may be obtained from:

SCIENTIFIC AND TECHNICAL INFORMATION DIVISION

NATIONAL AERONAUTICS AND SPACE ADMINISTRATION

Washington, D.C. 20546